20

Hessian Matrix-Based Shape Extraction and Volume Growing for 3D Polyp Segmentation in CT Colonography

Mark L. Epstein, MS, Ivan Sheu, BS and Kenji Suzuki, PhD
Department of Radiology, Division of Biological Sciences, The University of Chicago
USA

1. Introduction

The size of a lesion is one of the most important features for medical decision-making. The lesion size is usually measured by a clinician, and existing practice relies on size representation using the single longest dimension. There are, however, established variations among clinicians in manual measurement of lesion size, and a recent study implies volume measurement to be more clinically informative than the linear representation (Pickhardt et al., 2005). Volume metrics captures the real growth, and changes in size are amplified compared to those in one dimension. As a further hurdle, modern medical imaging systems produce images on which a polyp appears in a series of 2D slices -- measuring a lesion volume by drawing contours on many medical images is labor-intensive, poorly reproducible, and subjective. An automated volume measurement scheme has the potential to improve efficiency, consistency, and objectivity, avoiding problems of fatigue, variations in hand-eye coordination and subjective decision-making.
Colon cancer is the second leading cause of cancer deaths in the United States (Jemal et al., 2008). In the screening for this disease, lesion size plays an especially important role in determining malignant potential and the need for intervention. In particular, tracking a change in polyp size is an important marker for the clinician. Computed tomography colonography (CTC) is a diagnostic examination that radiologists use for detecting colonic polyps (precursor of colon cancer) (Macari & Bini, 2005). Significantly, the measured size of a polyp at CTC directs clinical treatment, by determining whether results of screening require intervention (Pickhardt et al, 2003). For instance, the current clinical standard is to weigh polyps ≥ 10 mm more highly. However, current measurement of the single longest dimension of a polyp is subjective and has variations among radiologists. As evidence of the variability of manual linear measurement of polyps at CTC, studies reported interobserver and intraobserver variations between 16 to 40% (Yeshwant et al., 2006; Taylor et al., 2006; Jeong et al., 2008). As stated earlier, volume measurement could be more clinically informative than longest linear dimension, and this holds true in CTC. However, manual measurement of polyps at CTC suffers from the same inherent problems as lesions in general (labor intensity, poor reproducibility, and subjectivity), and similarly would benefit from automation. As a medical sign frequently occurring in the population, a consistent and

efficient volume metric for polyps at CTC to inform clinical decisions is especially important.
Our purpose in this study was to develop a computerized scheme for segmenting 3D polyps in CTC and evaluate its accuracy and efficiency relative to "gold-standard" volumes determined by manual segmentation.

2. CT Colonography Database

Our CTC database (Table 1) was obtained from a multi-center clinical trial (DC Rockey, et al., The Lancet 2005). Our database consisted of 34 polyp views (17 polyps) in CTC scans from 15 patients. Each patient was scanned in both supine and prone positions with collimations of 1.0-2.5 mm. The image matrix size is 512 x 512 pixels with pixel sizes of 0.5 – 0.7 mm/pixel. Polyp locations were confirmed with reference to optical colonoscopy reports. Polyps were selected by a radiologist with the inclusion criteria of no fuzzy border and being visible in both supine and supine. The mean polyp size at optical colonoscopy was 10 mm, with 10 polyps in a 6-9 mm range, and 7 polyps in a 10-18 mm range.

Table 1. CT Colonography Database (DC Rockey, et al., The Lancet 2005)

Institutions	6 hospitals in the U.S.
Patients	15
Polyps	17 (34 views)
CT system	Multi-detector-row CT system
Slice thickness	1.0 – 2.5 mm
Image matrix size	512 x 512 pixels (0.5 – 0.7 mm/pixel)
Polyp location confirmation	With reference to optical colonoscopy reports
Inclusion criteria	No fuzzy border, visible on supine & prone
Polyp size	Mean 10 mm, 6 – 9 mm (n = 10), 10 – 18 mm (n = 7)

3. Establishment of the "Gold Standard"

Here is our protocol for establishing the "gold standard". A radiologist manually outlined the polyp in each 2D axial slice. High quality magnification enabled drawing precise contours. Volumes were calculated by summation of the enclosed areas. Three measurements were made, each at least one week apart, to reduce a memory effect bias. The average of the three trials was used as the "gold standard". Furthermore, the prone and supine volumes were averaged for the purposes of results analysis. An example of a manually outlined polyp is shown in Fig. 1.

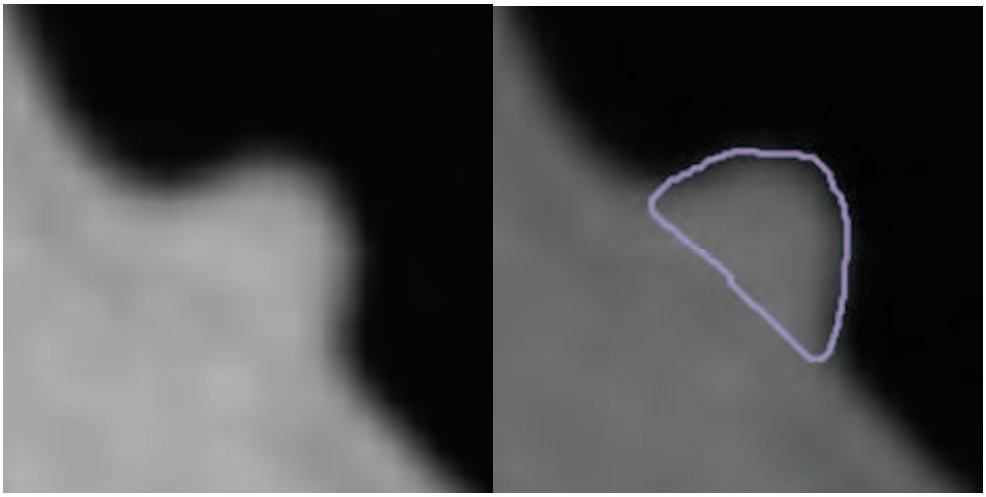

Fig. 1. Example of manually outlined polyp.

4. Automated Segmentation

A high-level flow chart of our automated polyp segmentation scheme is shown in Fig. 2. The scheme takes as input the CTC image data. The steps are: segmentation of the colon; extraction of a highly polyp-like seed region based on the Hessian matrix; segmentation of polyps by use of a 3D volume-growing technique; and sub-voxel refinement to reduce a bias of segmentation.

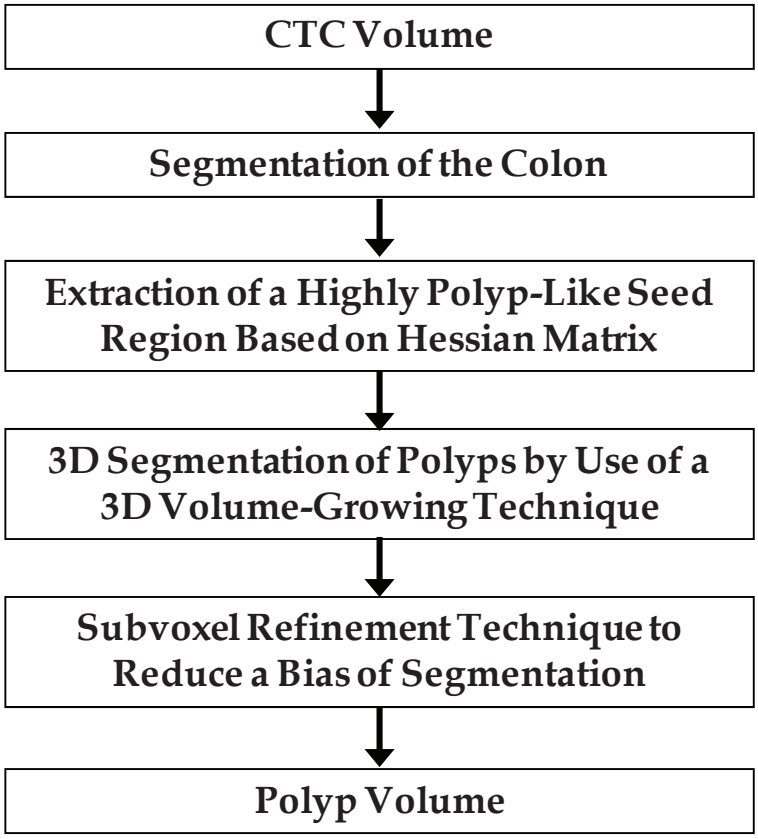

Fig. 2. Flow chart of our automated segmentation scheme.

A more detailed map of our segmentation scheme, showing sub-step intermediates, is given in Fig. 3. The reader is encouraged to refer to both the high-level flow chart and the detailed map while following the description of the scheme.

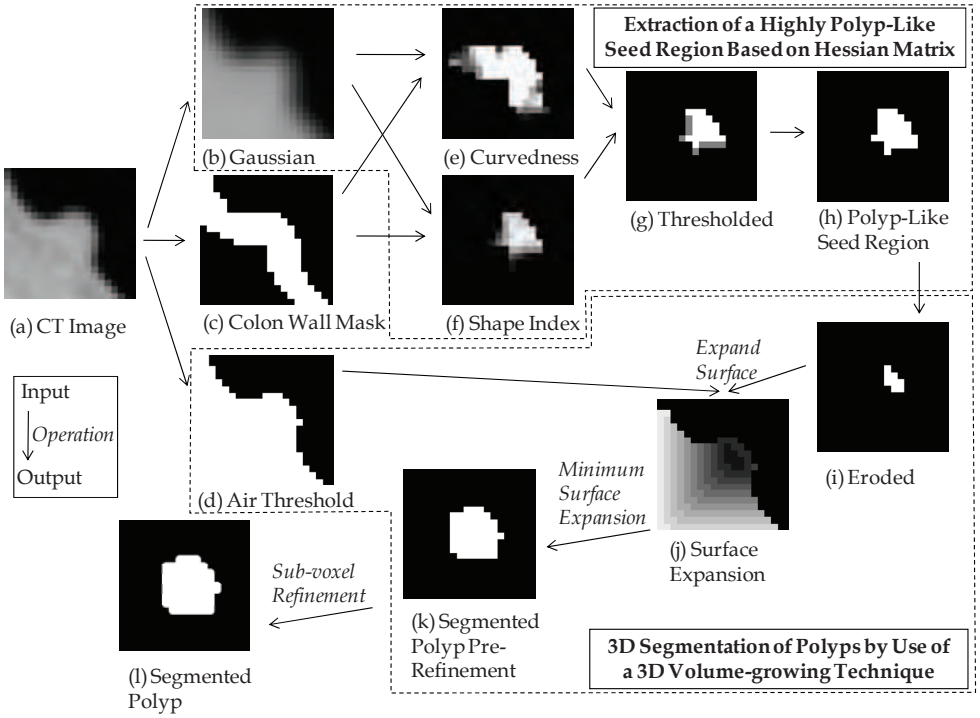

Fig. 3. Pictorial diagram of our segmentation algorithm.

The original 3D CT data are anisotropic such that an image voxel (i.e., a 3D pixel) is longer in the z direction than it is in the x and y directions. We account for this by generating isotropic 3D data (Fig. 3a). The isotropic volumes are generated by resampling the original 3D CT data through linear interpolation.

To confine our initial stages of polyp segmentation to the appropriate anatomical region, i.e., the colon, we next segment the colon wall with uniform thickness by using anatomical knowledge-based segmentation (Masutani et al., 2001; Yoshida et al., 2001) (Fig. 3c).

The next step of the scheme leverages the characteristic rounded shape of a bulbous polyp (Fig. 4 through Fig. 6). To reduce the effect of image noise, we apply a Gaussian smoothing filter (Fig. 3b). Our detection scheme relies on shape features; as an intermediate step, we apply a Hessian matrix operator which quantifies the local curvature in the 3D image (Dorai & Jain, 1997). The principal curvatures at a point describe the maximum and minimum rates that the local surface deviates from a plane. Two feature images can be derived from the principal curvatures, that together provide a measurement of the local shape and the "degree of the shape" at a point. These are known as shape index (Fig. 3f) and curvedness (Fig. 3e) (Yoshida et al., 2001). Shape index and curvedness are defined as

$$SI(p) \equiv \frac{1}{2} - \frac{1}{\pi} \arctan \frac{\kappa_1(p) + \kappa_2(p)}{\kappa_1(p) - \kappa_2(p)}, \tag{1}$$

$$CV(p) \equiv \sqrt{\frac{\kappa_1(p)^2 + \kappa_2(p)^2}{2}} \tag{2}$$

where κ_1, κ_2 represent the maximum and minimum curvatures, respectively. In this step, two feature images are created, whose quantities represent shape index and curvedness.

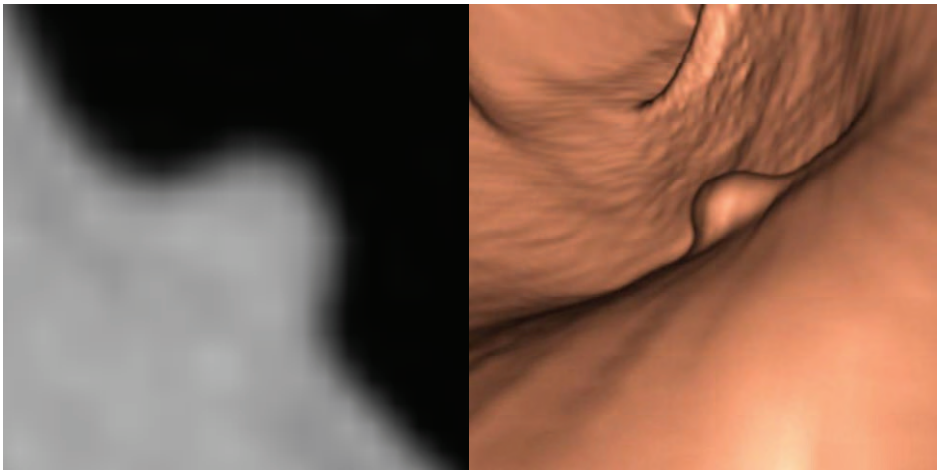

Fig. 4. Case 1 – polyp displayed in 2D axial and 3D endoluminal views.

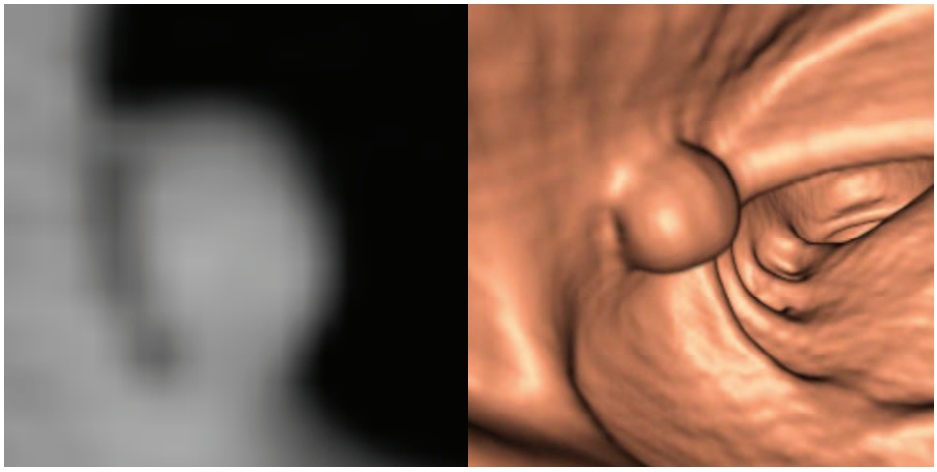

Fig. 5. Case 2 – polyp displayed in 2D axial and 3D endoluminal views.

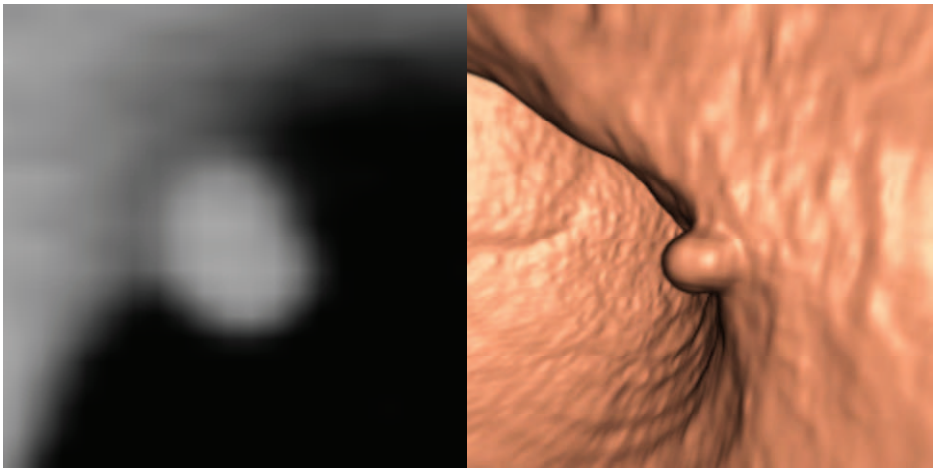

Fig. 6. Case 3 – polyp displayed in 2D axial and 3D endoluminal views.

The two Hessian matrix-based feature images are used together to extract a cap-shape structure that is typical of a bulbous polyp. To achieve this, first we run two range threshold operations on each feature images. The first range threshold is narrower than the second. The narrow range threshold operation results in a set or sets of very highly polyp-like voxels. The two narrow range threshold images are combined by a Boolean logical multiplication; the two wide range threshold images are similarly combined (Fig. 3g). We then perform a connectivity analysis based on a connected-component labeling algorithm, e.g., (Suzuki, Horiba et al., 2003; He, Chao, Suzuki et al., 2008) to allow the narrow range threshold region to grow to include any connected wider range threshold voxels. The result is a set of highly polyp-like regions localized on the cap-shape parts of polyps (Fig. 3h). A seed point may be manually provided by the user to select a single region of interest. Another way to envision the feature thresholding process is to think of the more relaxed range threshold operation as running first, and then eliminating regions which do not contain any voxels with values in the stricter range.

The polyp segmentation is still incomplete at this stage because the current region only includes the cap-shape region voxels that have the shape index and curvedness values within the designated range, such as the peripheral region of the polyp. For the next stage, we developed a segmentation technique based on region growing (Shapiro and Stockman 2001) to segment the remaining, non-cap-shape region. This stage of our segmentation algorithm is called 3D volume growing based on rate of lumen-prohibited expansion. First we employ an air threshold of the original CT image to distinguish the lumen from non-lumen (Fig. 3d). Second we load our seed region of highly polyp-like voxels obtained from the previous process (Fig. 3h). Third, we iteratively expand within the *non-lumen* for a predetermined 'k' number of iterations, while tracking the volume (Fig. 3j). Finally we find the region in which the volume expansion rate was the minimum (Fig. 3k). Expressed in set notation, the minimum volume expansion point occurs at the x^{th} iterative expansion when $\{W_x\} < \{W_i\}$ for i = 1, 2, ... k, where W is the set of expanded pixels.

The volume expansion rate minimum is chosen because this is the state where the polyp has been more completely segmented and it occurs before over-segmentation dominates. Up to

the volume expansion rate minimum, the surface expansion iterations are including nearby non-cap-shape voxels of the polyp. After the volume expansion rate minimum is reached, an ever-increasing volume expansion rate is observed while non-polyp voxels are added to the growing region. Therefore, the volume expansion rate minimum conveniently marks the transition in mode from inclusion of mainly polyp voxels to mainly non-polyp voxels. This point is best suited for capturing a region to proceed to the next stage of segmentation.

After collecting the gold standard and automated volumes, we determine that the automated volumes are on average smaller than the gold volumes. To reduce this bias of segmentation, we uniformly apply a 3D sub-voxel refinement technique (Fig. 3l and Fig. 7). The binary image shown represents a computer-segmented polyp. The grid lines indicate the original voxel size. First we resample the image to a higher resolution; a resampling factor of X, therefore, means that one original voxel is converted to X^3 voxels in the resampled image. Next we dilate the image by a specified radius, using a spherical kernel. The radius chosen was determined by the magnitude of the segmentation bias. The resulting region represents our computer-segmented polyp. Finally we calculate the volume, accounting for the resampling.

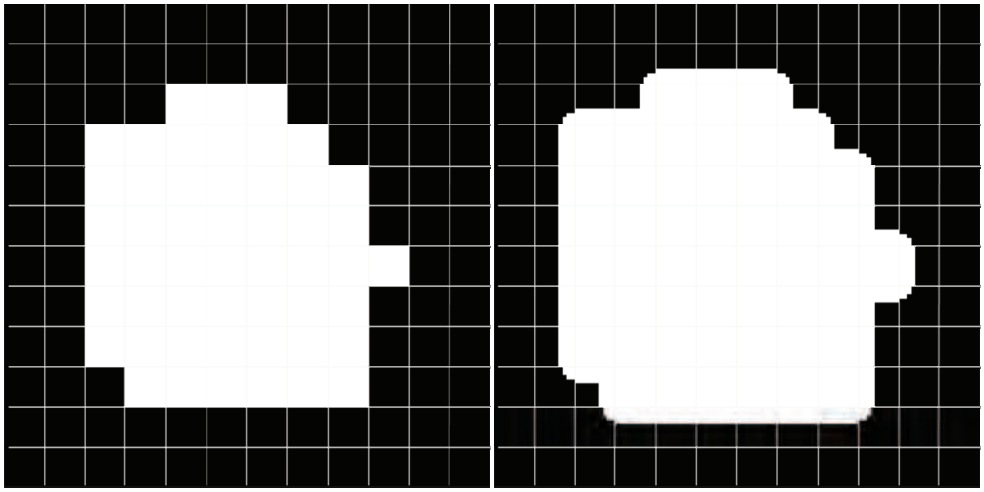

Input Output

Fig. 7. Illustration of the sub-voxel refinement.

5. Quantitative Analysis

Our measurement scheme yielded a mean polyp volume of 0.36 cc with a range of 0.15 to 1.24 cc, whereas the mean "gold standard" manual volume was 0.38 cc with a range of 0.14 - 1.08 cc (Table 2). The mean differences between automated and manual volumes for polyps ranging from 6-9 mm and those 10 mm or larger (by optical colonoscopy) were 23.4% and 17.5% with standard deviations (SD) of 19.2% and 17.6%, respectively (Table 3). These differences were comparable to the intra-observer variation of 14.0% with SD of 13.1%. The two volumetrics reached excellent agreement (intra-class correlation coefficient was 0.79) with no statistically significant difference (P = 0.61).

Table 2. Mean and range of volumes by automated and "gold-standard" manual segmentation

	Mean	Range
Manually traced volumes	0.38 cc	0.14 – 1.08 cc
Automated volumes	0.36 cc	0.15 – 1.24 cc

Table 3. Volume comparison between manual and automated segmentation; comparable to intra-observer variation of manual segmentation

	Mean ± SD
Absolute percent difference between automated and manual volumes for polyps 6-9 mm	23.4% ± 19.2%
Absolute percent difference between automated and manual volumes for polyps ≥ 10 mm	17.5% ± 17.6%
Intra-observer variation for manual volumes	14.0% ± 13.1%

6. Case Examples

Computer vs. manual contour comparison for Case 1 is shown in Fig. 8 for both supine and prone views. In this case, the automated volume is very close to the gold standard volume.

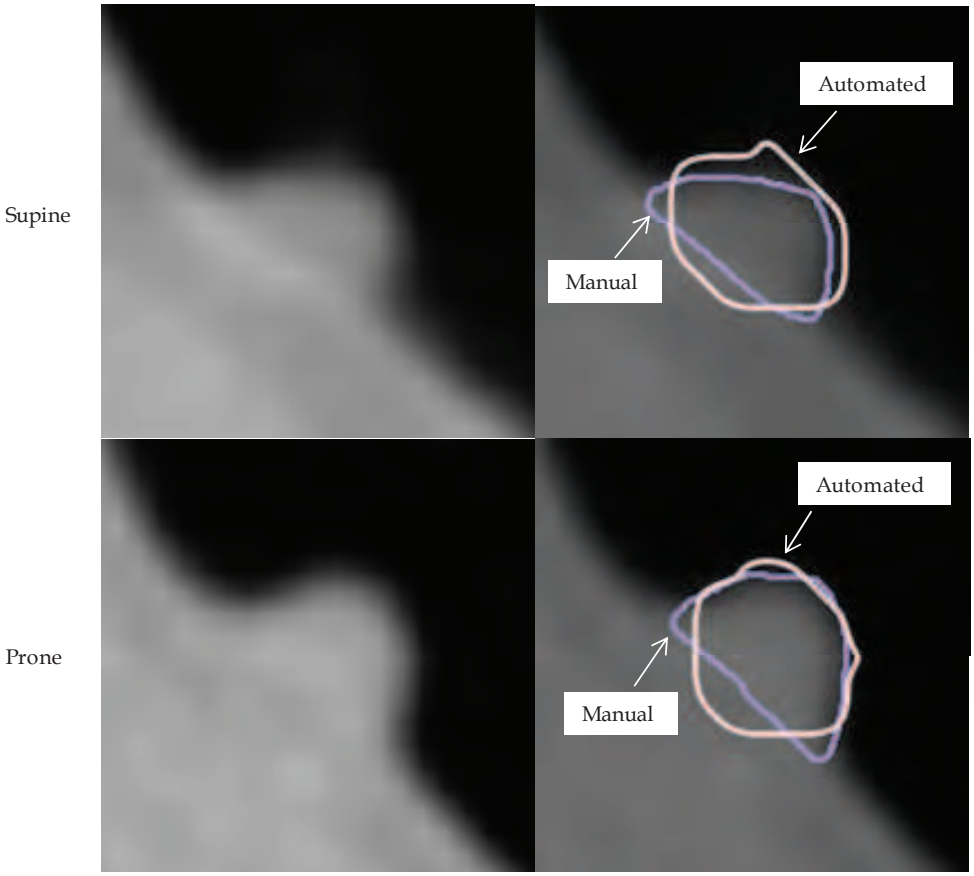

Fig. 8. Case 1: Comparison between automated and manual segmentation (prone "gold standard" manual volume = 0.21 cc; prone automated volume = 0.19 cc; supine "gold standard" manual volume = 0.15 cc; supine automated volume = 0.17 cc).

Computer vs. manual contour comparisons for two additional cases are shown in Fig. 9 and Fig. 10. The automated segmentation tended to include more of the low-intensity border at the colon-air interface, whereas it included less of the polyp's base than did the manual segmentation. The automated segmentation is fairly accurate for Cases 1 through 3.

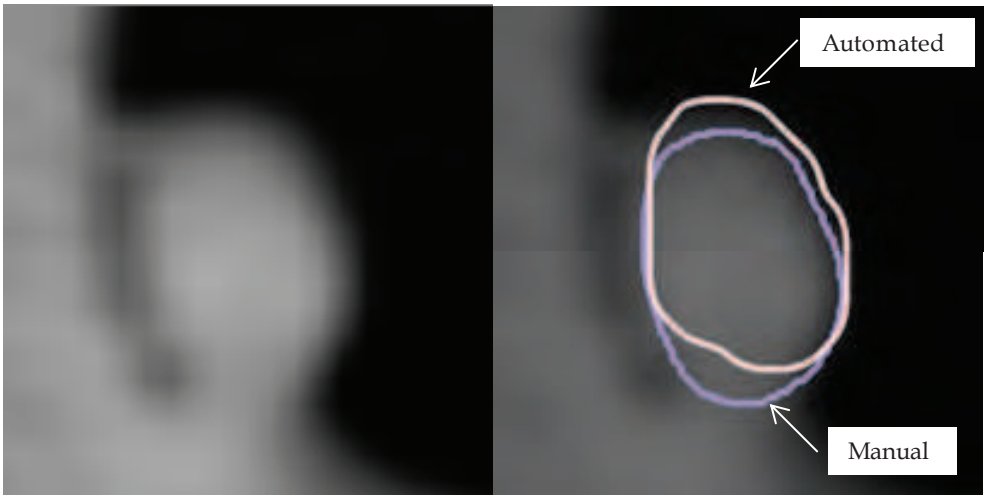

Fig. 9. Case 2 Prone: Comparison between automated and manual segmentation ("gold standard" manual volume = 0.34 cc; automated volume = 0.27 cc).

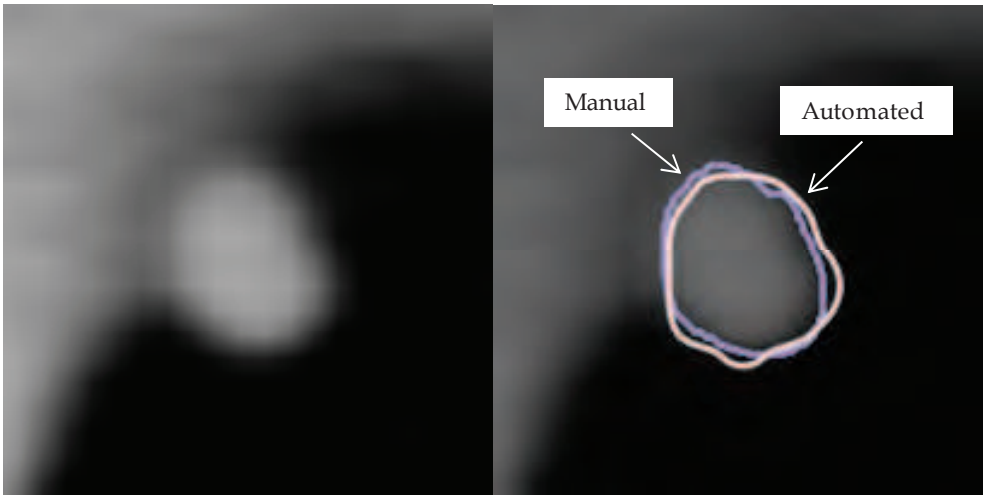

Fig. 10. Case 3 Supine: Comparison between automated and manual segmentation ("gold standard" manual volume = 0.17 cc; automated volume = 0.15 cc).

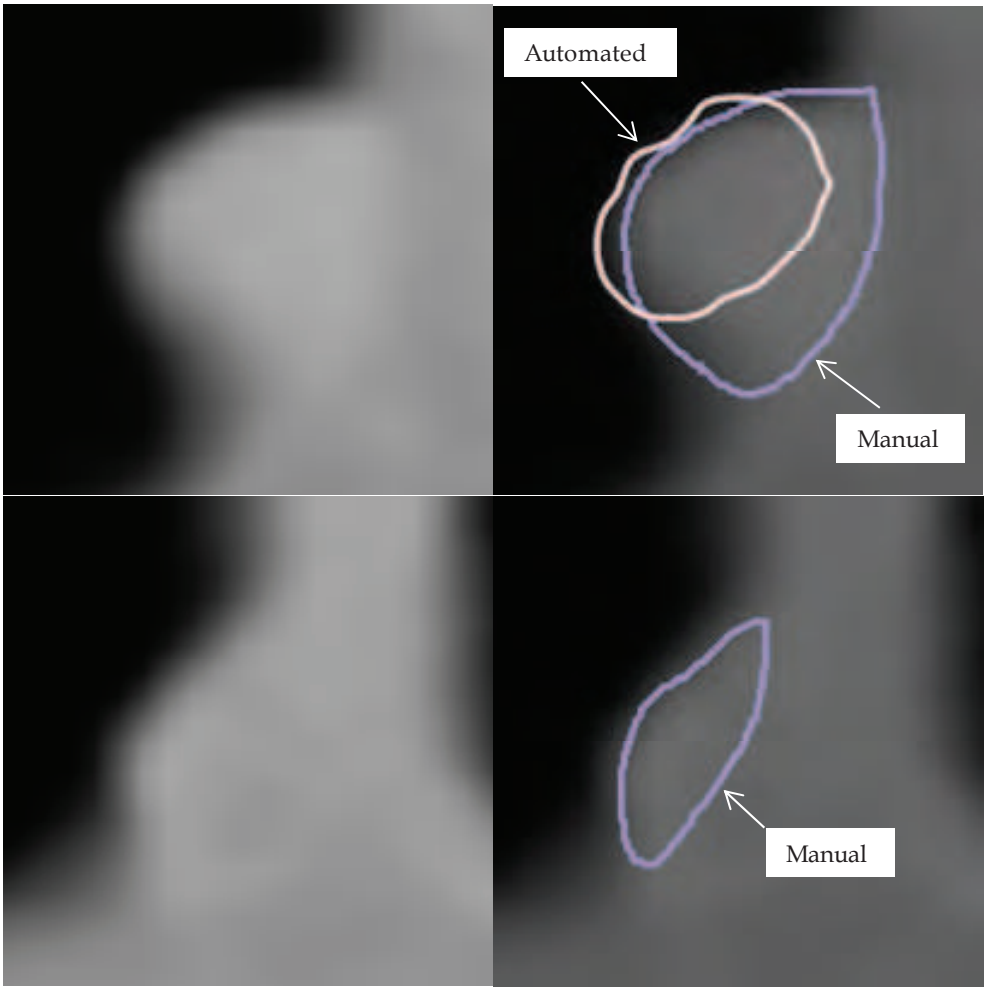

Fig. 11. Case 4 Prone: Example of under-segmentation by the automated segmentation, showing two slices ("gold standard" manual volume = 0.36 cc; automated volume = 0.19 cc).

Our algorithm may leave out parts of a polyp with indefinite borders or subtle morphology. An example of under-segmentation is represented by two slices of Case 4 in Fig. 11. In this polyp view, the computer under-segmented by missing part of the base and subtle peripheral regions.

We compared computer volumes against gold standard volumes and prone volumes against supine volumes and found generally good correlation. In the comparison of automated (computer) volume vs. "gold standard" manual volume, two outliers exist as a result of morphological features of the polyps: over-segmentation and under-segmentation. In the under-segmentation case, the bulb of a large, pedunculated polyp rested on the colon wall. In the over-segmentation case was an oblong, sessile polyp on a haustral fold.

In the comparison of prone vs. supine volumes of computer-segmented polyps, although the correlation is generally good, the two most significant outliers are caused by a change of polyp shape between the two patient positions. These polyps appear more bulbous in one view, and thus the segmentation is more accurate, but they appear subtler in the other view, which results in under-segmentation.

7. Conclusion

To put it in perspective, the advantages over manual volumetry are that an automated process is efficient, objective, and consistent, with one mouse click versus five minutes of manual drawing.

A limitation of automated volumetry is that the process occasionally results in mis-segmentation. This requires manual modification to fix, but it may retain some efficiency benefit within a semi-automated approach.

Polyp volumes obtained by our automated scheme agreed excellently with "gold standard" manual volumes. Our fully automated scheme efficiently can provide accurate polyp volumes for radiologists; thus, it would help radiologists improve the accuracy and efficiency of polyp volume measurements in CTC. Our scheme is potentially applicable to accurately segmenting 3D bulbous objects in 3D volumes.

Combining automated volume measurement with computer-aided detection of polyps (Suzuki, Yoshida et al., 2006; Suzuki, Yoshida et al., 2008) would provide radiologists even more efficient and accurate way of detection of polyps in CTC.

8. Acknowledgements

This study was supported by: The University of Chicago Cancer Research Center Support Grant; Grant Number R01CA120549 from the National Cancer Institute/National Institutes of Health, and SIRAF Cluster Funding in research.

9. References

Dorai, C; Jain, A.K (1997). "COSMOS – A Representation Scheme for 3D Free-Form Objects", *IEEE Transactions on Pattern Analysis and Machine Intelligence* 19(10):1115-1130.

He, L., Y. Chao, et al. (2008). "A run-based two-scan labeling algorithm." *IEEE Trans Image Process* 17(5): 749-56.

Jemal, A.; Siegel, R.; Ward, E.; Hao, Y.; Xu, J.; Murray, T.; Thun, M.J. (2008). "Cancer Statistics, 2008", *CA – A Cancer Journal for Clinicians* 58(2):71-96.

Jeong, J.Y.; Kim, M.J.; Kim, S.S. (2008). "Manual and Automated Polyp Measurement: Comparison of CT Colonography With Optical Colonoscopy", *Academic Radiology* 15(2):231-239.

Macari, M.; Bini, E.J. (2005). "CT colonography: Where have we been and where are we going?" *Radiology* 237(3):819-833.

Masutani, Y.; Yoshida, H.; MacEneaney, P.M.; Dachman, A.H. (2001). "Automated Segmentation of Colonic Walls for Computerized Detection of Polyps in CT Colonography", *Journal of Computer Assisted Tomography* 25(4):629-638.

Pickhardt, P.J.; Choi, J.R.; Hwang, I.; Butler, J.A.; Puckett, M.L.; Hildebrandt, H.A.; Wong, R.K.; Nugent, P.A.; Mysliwiec, P.A.; Schindler, W.R. (2003). "Computed Tomographic Virtual Colonoscopy to Screen for Colorectal Neoplasia in Asymptomatic Adults", *The New England Journal of Medicine* 349(23):2191-2200.

Pickhardt, P.J.; Lehman, V.T.; Winter, T.C.; Taylor, A.J. (2005). "Polyp Volume Versus Linear Size Measurements at CT Colonography: Implications for Noninvasive Surveillance of Unresected Colorectal Lesions", *Gastrointestinal Imaging* 186(6):1605-1610.

Shapiro, L. G. and G. C. Stockman (2001). Computer Vision. New Jersey, Prentice-Hall: 279-325.

Suzuki, K.; I. Horiba; Sugie, N.. (2003). "Linear-time connected-component labeling based on sequential local operations." *Computer Vision and Image Understanding* 89(1): 1-23.

Suzuki, K., H. Yoshida, et al. (2006). "Massive-training artificial neural network (MTANN) for reduction of false positives in computer-aided detection of polyps: Suppression of rectal tubes." *Med Phys* 33(10): 3814-24.

Suzuki, K., H. Yoshida, et al. (2008). "Mixture of expert 3D massive-training ANNs for reduction of multiple types of false positives in CAD for detection of polyps in CT colonography." *Med Phys* 35(2): 694-703.

Taylor, S.A.; Slater, A.; Halligan, S.; Honeyfield, L.; Roddie, M.E.; Demeshski, J.; Amin, H.; Burling, D. (2006). *Radiology* 242(1):120-128.

Yeshwant, S.C.; Summers, R.M.; Yao, J.; Brickman, D.S.; Choi, J.R.; Pickhards, P.J (2006). "Polyps: Linear and Volumetric Measurement at CT Colonography", *Radiology* 241(3):802-811.

Yoshida, H. and J. Nappi (2001). "Three-dimensional computer-aided diagnosis scheme for detection of colonic polyps." *IEEE Trans Med Imaging* 20(12): 1261-74.

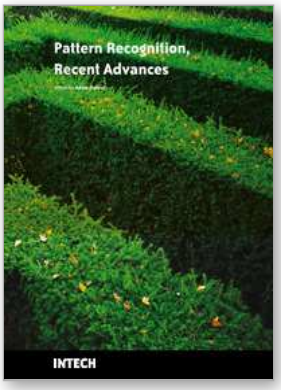

Pattern Recognition Recent Advances

Edited by Adam Herout

ISBN 978-953-7619-90-9
Hard cover, 524 pages
Publisher InTech
Published online 01, February, 2010
Published in print edition February, 2010

Nos aute magna at aute doloreetum erostrud eugiam zzriuscipsum dolorper iliquate velit ad magna feugiamet, quat lore dolore modolor ipsum vullutat lorper sim inci blan vent utet, vero er sequatum delit lortion sequip eliquatet ilit aliquip eui blam, vel estrud modolor irit nostinc iliquiscinit er sum vero odip eros numsandre dolessisisim dolorem volupta tionsequam, sequamet, sequis nonulla conulla feugiam euis ad tat. Igna feugiam et ametuercil enim dolore commy numsandiam, sed te con hendit iuscidunt wis nonse volenis molorer suscip er illan essit ea feugue do dunt utetum vercili quamcon ver sequat utem zzriure modiat. Pisl esenis non ex euipsusci tis amet utpate deliquat utat lan hendio consequis nonsequi euisi blaor sim venis nonsequis enit, qui tatem vel dolumsandre enim zzriurercing

How to reference

In order to correctly reference this scholarly work, feel free to copy and paste the following:

Mark L. Epstein, Ivan Sheu and Kenji Suzuki (2010). Hessian Matrix-Based Shape Extraction and Volume Growing for 3D Polyp Segmentation in CT Colonography, Pattern Recognition Recent Advances, Adam Herout (Ed.), ISBN: 978-953-7619-90-9, InTech, Available from: http://www.intechopen.com/books/pattern-recognition-recent-advances/hessian-matrix-based-shape-extraction-and-volume-growing-for-3d-polyp-segmentation-in-ct-colonograph

INTECH
open science | open minds

InTech Europe
University Campus STeP Ri
Slavka Krautzeka 83/A
51000 Rijeka, Croatia
Phone: +385 (51) 770 447
Fax: +385 (51) 686 166
www.intechopen.com

InTech China
Unit 405, Office Block, Hotel Equatorial Shanghai
No.65, Yan An Road (West), Shanghai, 200040, China
中国上海市延安西路65号上海国际贵都大饭店办公楼405单元
Phone: +86-21-62489820
Fax: +86-21-62489821